sustainability

MDPI

Article

Long-Term Prediction of Hydrometeorological Time Series Using a PSO-Based Combined Model Composed of EEMD and LSTM

Guodong Wu [1,2], Jun Zhang [2,*] and Heru Xue [1,*]

[1] College of Computer and Information Engineering, Inner Mongolia Agricultural University, Hohhot 010026, China; ndwgd@imau.edu.cn
[2] College of Science, Inner Mongolia Agricultural University, Hohhot 010018, China
* Correspondence: zj325328333@163.com (J.Z.); xuehr@126.com (H.X.)

Abstract: The accurate long-term forecasting of hydrometeorological time series is crucial for ensuring the sustainability of water resources, environmental conservation, and other related fields. However, hydrometeorological time series usually have strong nonlinearity, non-stationarity, and complexity. Therefore, it is extremely challenging to make long-term forecasts of hydrometeorological series. Deep learning has been widely applied in time series prediction across various fields and exhibits exceptional performance. Among the many deep learning techniques, Long Short-Term Memory (LSTM) neural networks possess robust long-term predictive capabilities for time series analysis. Signal decomposition technology is utilized to break down the time series into multiple low complexity and highly stationary sub-sequences, which are then individually trained using LSTM before being reconstructed to generate accurate predictions. This approach has significantly advanced the field of time series prediction. Therefore, we propose an EEMD-LSTM-PSO model, which employs Ensemble Empirical Mode Decomposition (EEMD), to decompose the hydrometeorological time series and subsequently construct an LSTM model for each component. Furthermore, the Particle Swarm Optimization (PSO) algorithm is utilized to optimize the coefficients and reconstruct the final prediction outcomes. The performance of the EEMD-LSTM-PSO model is evaluated by comparing it with four other models using four evaluation indicators: root mean square error (RMSE), mean absolute percentage error (MAPE), correlation coefficient (R), and Nash coefficient (NSE) on three real hydrometeorological time series. The experimental results show that the proposed model exhibits exceptional performance compared with the other four models, and effectively predicts long-term hydrometeorological time series.

Keywords: time series; hydrometeorological elements; long-term prediction; EEMD; LSTM; PSO

Citation: Wu, G.; Zhang, J.; Xue, H. Long-Term Prediction of Hydrometeorological Time Series Using a PSO-Based Combined Model Composed of EEMD and LSTM. *Sustainability* **2023**, *15*, 13209. https://doi.org/10.3390/su151713209

Academic Editors: Lifeng Wu and Shenming Fu

Received: 27 June 2023
Revised: 30 August 2023
Accepted: 31 August 2023
Published: 3 September 2023

1. Introduction

The adverse impacts of climate change present a formidable challenge to sustainable development [1,2]. Precise long-term forecasting information empowers decision-makers at all levels to strategize for adaptation to climate change across diverse sectors, including agriculture, healthcare, tourism, and forestry [3]. Hydrometeorology plays a crucial role in promoting sustainable development [4], thus necessitating the enhancement of forecast quality through diverse approaches and the in-depth exploration of various natural phenomena to optimize hydrometeorological predictions. The prediction of runoff and precipitation is a fundamental aspect of hydrology and water resources, serving as the cornerstone for the scientific planning, rational allocation, and adaptive utilization of water resources. Accurate prediction holds great significance in enabling stakeholders within river basins to develop scientifically informed water use plans that promote sustainable development [5,6].

At regional and global scales, drought is one of the most important factors affecting the resilience of terrestrial ecosystems [7]. Anderegg et al. [8] found that, in recent years, the decrease in the Amazon rainforest ecosystem diversity and the decrease in the carbon sink are related to the increase in the degree of drought. Dannenberg et al. [9] found that the global temperature may continue to increase in the future, which will lead to more frequent and stronger drought disasters. Accurate prediction can help people understand the changes in hydrological and meteorological elements in the future, and help implement the necessary measures in order to maintain the stability and sustainable development of the ecosystem, thus promoting regional carbon sinks.

Due to the non-stationary and nonlinear nature of hydrometeorological elements, the task of improving the prediction accuracy faces significant challenges. Therefore, the prediction of hydrometeorological elements has received significant attention [10–13]. Researchers have developed a variety of forecasting models for hydrometeorological elements, which can generally be divided into two categories: physical models and data-driven models. Physical models are based on model-driven numerical simulations of hydrometeorological processes. The distributed hydrological model is one of the most successful and widely used physical models, such as SWAT (Soil and Water Assessment Tool) [14], VIC (Variable Infiltration Capacity) [15], and TOPMODEL (Topography-based hydrological MODEL) [16]. However, the building of a distributed hydrological model needs many physical parameters from topography, soil type, soil thickness, solar radiation, and hydrometeorological data [17]. It is difficult to obtain these data because they require a lot of human financial resources. In addition, the physical model is more dependent on the mechanism process, so the modeling has great uncertainty. Data-driven models only need to consider input data and output data, but do not need to clarify the mechanism of hydrometeorology. Data-driven models can simplify complex problems, streamline the modeling process, and facilitate the in-depth exploration of internal data relationships. This approach is particularly effective for hydrologic forecasting in areas with limited data availability. Therefore, data-driven models open a new way for the evaluation and prediction of hydrometeorological elements. Data-driven models can be divided into three categories which include statistical models, neural network models, and combinatorial models.

A standard statistical model is the Box–Jenkins model, which mainly deals with stationary time series and fits an Autoregressive Moving Average (ARMA), Autoregressive Integrated Moving Average (ARIMA) or Seasonal Autoregressive Integrated Moving Average (SARIMA) model [18–20].

The artificial neural network (ANN) is another data-driven model that is widely used in hydrometeorological research due to its powerful nonlinear data processing capability [21–26]. However, a single ANN model also has shortcomings, such as the slow response of the gradient descent learning algorithm and the unsatisfactory processing effect on the mutation points in the data. Long Short-Term Memory (LSTM) [27] is one of the more successful RNNs. LSTMs prevent gradient vanishing or exploding by adding "gate" units and can effectively capture the internal dynamic features of nonlinear time series [28]. Kratzert et al. constructed an LSTM network for daily rainfall and runoff simulations. The results showed that it achieved competitive results compared to the Sacramento soil moisture calculation model [29]. Widiasari et al. established an LSTM neural network model to predict floods, and the accuracy of the results was higher than that of multiple linear regression [30]. Xiang et al. established an LSTM neural network model from rainfall observation, rainfall forecast, runoff observation, and monthly evapotranspiration data to predict the hourly runoff within 24 h. The model's accuracy is better than that of linear regression, Lasso regression, Ridge regression, support vector regression, and Gaussian Process Regression. It is also found that LSTMs can improve the accuracy of short-term flood forecasting [31]. The continuous development and updating of neural network algorithms and structures provide reliable data-driven model selection for various researchers.

The combinational model combines the individual models according to certain rules, which captures more comprehensive information than individual models to improve the prediction accuracy [32]. There is a way to combine the signal decomposition technique and the prediction model in series. The Fourier decomposition method, wavelet decomposition method, and empirical mode decomposition (EMD) are standard and widely applied to process sequence data. EMD can adaptively decompose a non-stationary time series into several relatively stationary components with different frequencies. In 2009, Wu [33] proposed Ensemble Empirical Mode Decomposition (EEMD) to solve the mode mixing phenomenon of EMD, which further promoted the application of the technology in various fields. Wang et al. used EEMD decomposition technology to improve the prediction accuracy of ARIMA in annual runoff data [34] and combined EEMD technology with ANN to improve the long-term prediction accuracy of annual runoff [35]. Introducing EEMD decomposition technology into other commonly used prediction models can enhance the prediction accuracy of hydrometeorological time series. Moreover, in terms of the reconstruction method, most scholars still directly add the prediction results of the EEMD components to obtain the final prediction results.

The swarm intelligence optimization algorithm has opened a new path for solving optimization problems. The swarm intelligence optimization algorithm has the characteristics of a simple principle and easy implementation and can solve complex nonlinear optimization problems. Particle swarm optimization (PSO) is an efficient and fast convergence swarm optimization algorithm. PSO has apparent advantages in solving continuity problems, so it is widely used in parameter optimization [36–38].

The purpose of this paper is to build a decomposition–predict–integration predictive model, denoted as EEMD-LSTM-PSO, which can be effectively employed for the long-term forecasting of hydrometeorological time series. Our objective is to enhance the predictive accuracy of hydrological and meteorological variables, enabling proactive forecasting and facilitating sustainable development in ecological environment, water resources, and related domains.

The structure of this paper is arranged as follows. Section 2 briefly introduces the basic principles of EEMD, LSTM, and PSO, explains the construction of the EEMD-LSTM-PSO model, and describes the preliminary settings of the three basic methods. Section 3 presents the experimental process of the EEMD-LSTM-PSO model. Section 4 compares the model with the ARIMA, LSTM, EEMD-LSTM, and EEMD-LSTM-MLR models according to four indicators. Section 5 and 6 discusses the results and summarizes the conclusions.

2. Methods

2.1. Method for Signal Decomposition

EMD is a multi-scale signal decomposition method proposed by Huang et al. [39]. It is mainly used to analyze nonlinear, non-stationary, and complex time series data, such as images [40], sounds [41], seismic data [42], meteorological data [43], and other signal processing. In essence, this method smooths a signal, decomposes the components of different scales from the original signal, and obtains a series of Intrinsic Mode Function (IMF) components containing local feature information. Compared with traditional time series decomposition methods (such as wavelet decomposition), the EMD is locally adaptive. Instead of relying on any prior basis function, according to the fluctuation characteristics of the data, it decomposes the time series into IMFs and residuals of different frequencies.

The IMFs in the algorithm need to satisfy two conditions:

1. In the entire data sequence, the number of extreme points (i.e., local maximum points and local minimum points) is equal to the number of zero-crossing points or difference 1;
2. The mean of the upper and lower envelopes is 0.

The basic idea of the EMD algorithm is to regard time series data as a function composed of multiple wave modes and to decompose these different wave functions one by one through a special screening process. Denoting the original time series data as $x(t)$,

$t = 1, 2, 3, \ldots, m$, m is the length of the series. The specific process of the EMD method is as follows:

1. Let iteration $i = 1$, and $d_{i=1}(t) = x(t)$.
2. Find out all the local maximums and minimums of $d_i(t)$. Interpolate and calculate the upper envelope $e_{max}(t)$ using local maximums and lower envelope $e_{min}(t)$ and using local minimums. Calculate their mean $m_i(t) = (e_{max}(t) + e_{min}(t))/2$.
3. Let $h_i^1(t) = d_i(t) - m_i(t)$, and determine whether it satisfies both conditions in the IMF definition. If true, then $h_i^1(t)$ is the ith $IMF_i(t)$ and let $d_{i+1}(t) = d_i(t) - IMF_i(t)$. Otherwise, $d_i(t) = h_i^1(t)$.
4. Repeat steps (2) and (3) until $d_i(t)$ becomes monotonic or the number of extreme points in the envelopes is equal to or less than 3.

After the above process, the original time series is finally decomposed into several IMFs and a residual sequence.

$$x(t) = \sum_{i=1}^{N} IMF_i(t) + Res(t),\ t = 1, 2, 3, \ldots, m. \quad (1)$$

where $Res(t)$ is the residual item that contains the main trends of the original sequence.

The decomposition of the signal can vary significantly due to modal mixing. In response to this problem, Huang et al. proposed a noise-assisted data analysis method based on EMD in 2004, called EEMD, the idea of which is to add white noise with limited amplitude to the signal and define the IMF as the mean value of the sets. Therefore, the EEMD algorithm can be considered as adding white noise to EMD. It is generally assumed that the added white noise follows a normal distribution with a mean of 0 and a standard deviation of ε. The steps of EEMD are as follows:

1. Add white noise to the subject sequence.
2. Using the EMD to decompose the new data sequence with added white noise, a series of IMFs are obtained.
3. Adding different white noise to the original series, repeat the above two steps for N times. N groups of different decomposition results are obtained.
4. Take the average of all IMF components as the result.

2.2. Method for Components Forecasting

An artificial intelligence model can overcome drawbacks like the serial correlation and non-linearity of conventional forecasting methods such as ARMA and ARIMA. Recurrent neural networks (RNNs) can handle arbitrarily long sequences. However, this is not the case in practice because the RNN structure is prone to gradient vanishing and gradient exploding. To overcome those limitations of traditional RNNs, Hochreite and Schmidhuber [27] proposed an improved version of RNNs, called LSTMs. LSTMs can effectively deal with the "long-term dependency" problem in RNNs, which can capture deeper connections in the sequences. Therefore, in recent years, LSTM has been widely used in time series forecasting [44,45].

Compared with the traditional RNNs, the basic unit of the hidden layer of LSTM is a memory block, which contains memory neurons and three gates, namely the input gate, forget gate, and output gate. These three gates regularize the flow of information into and out of memory neurons. The input gate controls the input of information into the activation function of the memory neuron. The forget gate controls the information at the current time step to be remembered or forgotten. It can filter information, keep useful information, and discard useless information.

So, the mathematical expression corresponding to the LSTM structure is as follows [46]:

$$\begin{cases} i_t = \sigma(\omega_{xi}x_t + \omega_{hi}h_{t-1} + \omega_{ci}c_{t-1} + b_i) \\ f_t = \sigma(\omega_{xf}x_t + \omega_{hf}h_{t-1} + \omega_{cf}c_{t-1} + b_f) \\ c_t = f_t \cdot c_{t-1} + i_t \cdot \tanh(\omega_{xc}x_t + \omega_{hc}h_{t-1} + b_c) \\ o_t = \sigma(\omega_{xo}x_t + \omega_{ho}h_{t-1} + \omega_{co}c_{t-1} + b_o) \\ h_t = o_t \cdot \tanh(c_t) \\ y_t = \omega_{hy}h_t + b_y \end{cases}, \quad (2)$$

where x_t is the input; y_t is output; i_t, f_t, o_t and c_t are the input gate, forget gate, output gate, and memory neuron, respectively; b_i, b_f, b_o, and b_c are the corresponding thresholds, respectively; σ is the sigmoid function; w_x represents the difference between the input node and the hidden node; w_h represents the weight between the hidden node and the memory neuron; and w_c is the weight connecting the memory neuron to the output node.

2.3. Method for Optimization of Reconstruction Coefficients

A time series is decomposed into several subsequences by EEMD. Each subsequence will be predicted by applying LSTM and a forecasting result achieved. In several studies, the prediction of the original time series is obtained by adding the predicted values of all the subsequences, which means that the coefficients are all equal to 1.

According to the principle of EEMD, a zero-mean white noise is introduced into the target data series, which is then decomposed into N IMFs: IMF_1, IMF_2, …, IMF_N. After M repetitions, let $IMF_i = \frac{1}{M}\sum_{k=1}^{M} {IMF_i}^{<k>}$, where ${IMF_i}^{<k>}$ denotes the IMF_i and follows the completion of the M-th operation. In fact, it should be $IMF_i = \lim_{M\to\infty} \frac{1}{M}\sum_{k=1}^{M} {IMF_i}^{<k>}$. Therefore, in practical applications, Formula (1) is not strictly applicable due to the finite value of M. Furthermore, the prediction accuracy of individual IMF components varies, particularly with higher frequency components exhibiting greater prediction errors. Therefore, the direct summation for reconstructing the predicted value of the target data series may result in significant inaccuracies.

In the present study, we applied an intelligent algorithm to optimize the sum coefficients for obtaining more accurate prediction results. PSO [47,48] is a swarm intelligence optimization algorithm first proposed by Kennedy and Eberhart in 1995 based on research on bird predation behavior. The PSO algorithm can solve complex optimization problems and is widely used in many fields such as neural network training, parameter identification, function optimization, and power system optimization. Each particle in the algorithm represents a potential solution to the problem, and the characteristics of the particle are characterized by three indicators: position, speed, and fitness. The particle is in the solution space, and its position is updated by tracking the individual extremum and the population extremum. The individual extremum refers to the position with the best fitness among the positions experienced by the individual. And, the population extremum refers to the position with the best fitness of all particles in the population.

Suppose there is a population of particles in a d-dimensional space. In each iteration, the particle updates its velocity and position by computing individual and population extrema:

$$\begin{array}{l} V_i^{k+1} = wV_i^k + c_1r_1(P_i^k - X_i^k) + c_2r_2(P_g^k - X_i^k) \\ X_i^{k+1} = X_i^k + V_i^{k+1} \end{array}, \quad (3)$$

where w is the inertia weight; V is the particle velocity; c_1 and c_2 are two non-negative constants; r_1 and r_2 are random numbers distributed in [0,1]; i represents the i-th particle and t represents the current iterations; P_i^k is individual historical optima in the k-th iteration; and P_g^k is globe optima in the k-th iteration.

2.4. EEMD-LSTM-PSO Model

The model built in this paper is a combination model that integrates the data decomposition algorithm and the prediction model. EEMD does not require any subjective intervention and provides an adaptive approach to data analysis. By eliminating modal mixing, a set of IMFs is generated that can carry the full physical meaning of each component. EEMD can decompose the various time-frequency features in the time series data of the hydrometeorological elements one by one, which is convenient for further prediction and improves the prediction accuracy. LSTMs are a excellent alternative to RNNs, eliminating the risk of gradient vanishing and gradient exploding. When making predictions that do not consider underlying mechanistic processes, LSTM models can be used as an alternative to physical models for assessing changes in hydrometeorological elements. Moreover, the model structure of LSTM gives it a good long-term prediction ability. According to the literature review, there are few prediction studies based on the combined model of EEMD and LSTM in this field. Therefore, this paper attempts to construct a decomposition and integration model of EEMD-LSTM for empirical analysis and explore its performance in the long-term prediction of time series of hydrometeorological elements.

The basic idea of the prediction model in this paper contains three factors:

1. Use the EEMD decomposition to decompose the original data sequence into several IMFs and a trend term (residual);
2. Build LSTMs for every sequence from the above step;
3. Use the PSO algorithm to optimize the reconstruction coefficients to obtain the prediction results.

Figure 1 presents the structure of the proposed prediction model, namely EEMD-LSTM-PSO.

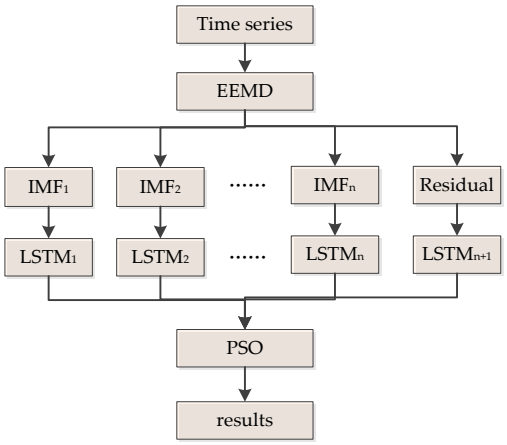

Figure 1. The structure of EEMD-LSTM-PSO model.

In the EEMD algorithm, the white noise added to the target time series obeys a normal distribution with a mean of 0 and a standard deviation of 0.1, and the number of repetitions is set to 100.

When using LSTM for time series forecasting, it involves setting the iteration time step (iteration) to describe the forecast period. The LSTM neural networks constructed in this paper all set the number of iterations to 1, which means that the previous record of the time series is used to predict the next one. Another essential parameter, 'epoch', is not set uniformly, but the optimal value is determined by repeated testing over and over again. The same treatment applies to the setting of the learning rate.

In addition, the loss function used in all LSTM neural networks in this paper is the mean square error function. In order to ensure an optimal network performance, enhance convergence speed, and prevent gradient explosion, it is imperative to normalize the input

data [45,49]. The normalization of the input data in this paper is carried out according to the following formula:

$$inputn = \frac{input - mean\_input}{v\_input}, \tag{4}$$

where *input* is the original input data, *mean_input* is the mean of the input data, and *v_input* is the standard deviation.

In this paper, the fitness function of the PSO algorithm is set as the Euclidean distance between the weighted sum and the corresponding observation sequence. If $\alpha_1, \alpha_2, \ldots, \alpha_{N+1}$ denote the coefficients to be optimized, the fitness function is

$$fitness = \left\| \left[\sum_{j=1}^{N} (\alpha_j \cdot IMF_j) + \alpha_{N+1} \cdot d(t) \right] - x(t) \right\|^2, \tag{5}$$

where IMF_j is the prediction results of the empirical modal component; $d(t)$ is the prediction of the residual term (or trend term); $x(t)$ is the corresponding observation value in the original sequence; and $\|\cdot\|$ is the Euclid norm [50].

We introduce the mutation operation in the PSO algorithm to improve search accuracy. The so-called mutation operation refers to re-initializing some variables according to a certain probability. It can expand the population search space in the iterative process and facilitate the search for particles in a larger space to avoid staying on local extrema. In the selection of the inertia weight for the particle velocity update, the linear decreasing weight is adopted to balance the global search ability and local search ability of PSO. It can be described as

$$w(k) = w_{start} - (w_{start} - w_{end}) \times k/\text{maxgen}, \tag{6}$$

where w_{start} is the initial inertia weight; w_{end} is the inertia weight whose iteration reaches the maximum number; k is the current iteration number; and *maxgen* is the maximum number of iterations. In this way, the inertia weight gradually decreases with the increasing number of iterations, which can ensure sufficient search capability. Generally, when $w_{start} = 0.9$ and $w_{end} = 0.4$, the algorithm has the best performance [51]. Thus, such a parameter configuration is adopted in our PSO algorithm.

2.5. Method for Model Evaluation

This paper selects four evaluation indicators: root mean square error (RMSE), mean absolute percentage error (MAPE), correlation coefficient (R), and Nash–Sutcliffe (NSE) to compare the effects of the three models.

RMSE is timescale-dependent, which is useful when comparing different methods applied to the same dataset. Prediction methods can make the RMSE of the prediction result smaller, generally producing smaller errors, but RMSE cannot be used to compare the prediction results between datasets of different scales. MAPE is a relative value, so it is not affected by scale, but infinity or undefinition occurs when the observed value is zero. Lower RMSE and MAPE can reflect higher model accuracy. The correlation coefficient is a statistical index to study the degree of linear correlation between two data vectors, and it is widely used in model evaluation in hydrometeorology. The value of the correlation coefficient is between -1 and 1. When it is close to 1, it indicates that the correlation between the predicted and the observed value is high, which can also be interpreted as their change trends being close. The Nash coefficient is a standard and powerful index to evaluate the accuracy of hydro-climate models, which was proposed by Nash and Sutcliffe in 1970 [52]. The range of the NSE coefficient is $(-\infty, 1]$. If NSE is close to 1, the model is of good quality and high reliability. If NSE is close to 0, this means that the prediction results are close to the average level of the observed values, and the results can be generally accepted as credible; but, if the prediction error is too large and the NSE is far less than 0,

this means that the model is untrustworthy. The calculation formulas of the four indicators are as follows:

$$\mathrm{RMSE} = \sqrt{\frac{\sum_{i=1}^{n} (E_i - O_i)^2}{n}}, \tag{7}$$

$$\mathrm{MAPE} = \frac{100}{n} \sum_{i=1}^{n} \left| \frac{E_i - O_i}{O_i} \right|, \tag{8}$$

$$\mathrm{R} = \frac{\sum_{i=1}^{n} (E_i - \overline{E})(O_i - \overline{O})}{\sqrt{\sum_{i=1}^{n} (E_i - \overline{E})^2 \sum_{i=1}^{n} (O_i - \overline{O})^2}} \tag{9}$$

$$\mathrm{NSE} = 1 - \frac{\sum_{i=1}^{n} (E_i - O_i)^2}{\sum_{i=1}^{n} (O_i - \overline{O})^2} \tag{10}$$

where E_i is the prediction, O_i is the observation, $\overline{E}$ is the mean of all predictions, and $\overline{O}$ is the mean of all observations.

According to the principle of majority voting, when the results of three or more indicators are better, we believe that the corresponding model has the highest prediction accuracy and the highest reliability.

3. Experiments

In this section, we selected hydrometeorological elements as experimental objects for the practice sequence and established the LSTM, EEMD-LSTM, EEMD-LSTM-PSO, and ARIMA models for comparison. To compare the optimization methods of the reconstruction coefficients, we also optimized the coefficients using multiple linear regression (MLR) to establish the EEMD-LSTM-MLR model. The efficiency of the model was evaluated using the four indexes in the previous section.

We selected data series with diverse hydrometeorological elements, varied geographical locations, and different time scales in order to conduct experiments and assess the predictive performance of our model. The three datasets comprise annual precipitation data for tropical regions, monthly precipitation data at a cold arid site, and annual runoff data from the upper tributaries of the Yellow River. We evaluate the model's performance on precipitation and runoff data at an annual time scale, as well as on precipitation data at different time scales.

The first dataset selected is annual runoff in the upper reaches of the Heihe River in China. The Heihe River is one of the tributaries of the Yellow River Basin, originating from the Minshan Mountains in Sichuan Province, China. The time series of annual runoff in the upper reaches of the Heihe River is from the National Glacier and Permafrost Desert Science Data Center (http://www.ncdc.ac.cn (accessed on 6 January 2021)), which is from 1000 to 2008. This paper selects a section from 1800 to 2008 as the research object. The maximum runoff of the intercepted time series is 2053.188 million m^3 in 1955, while the minimum value is 807.5158 million m^3 in 1824. The standard deviation is 229.081 million m^3. We select the first 190 items of data as the training set and the last 19 items of data as the test set.

The second dataset is the national average annual precipitation data from India (1871–2016). The dataset is from the Indian Institute of Tropical Meteorology (https://www.tropmet.res.in (accessed on 29 August 2017)) and is obtained by dividing India into 30 meteorological divisions and calculating the monthly average precipitation with the division area as the weights. This time series contains 146 items of data; the last 20 are used as the test set, and the rest are used as the training set. The maximum of the series is 1347.0 mm, while the minimum is 810.9 mm. The standard deviation is 101.0 mm.

The third dataset selected is the monthly precipitation data of the Xilin River Basin in China from January 1961 to December 2016. The purpose is to explore the prediction effect of the proposed model on monthly precipitation data with strong randomness. The Xilin River is located in China's Inner Mongolia Autonomous Region and is a typical arid and semi-arid grassland river in northern China. The annual precipitation in the Xilin River Basin is low and its time distribution is uneven. The annual precipitation is about 300 mm, mainly concentrated in June-August, and the maximum precipitation occurs in July each year. The collected time series contains 672 items of data. The maximum monthly precipitation is 204.0 mm, while the minimum monthly precipitation is 0.2 mm. The standard deviation of the time series is 31.5 mm. The current study uses the last 36 months of data as the test set and the rest as the training set.

We separately constructed EEMD-LSTM-PSO models to facilitate the long-term prediction of the three time series and to calculate the corresponding root mean square error (RMSE). To assess the impact of introducing EEMD on the prediction accuracy of LSTM, we also trained single LSTM and ARIMA models for these three time series. Furthermore, in order to compare reconstruction coefficient optimization strategies, we additionally developed EEMD-LSTM and EEMD-LSTM-MLR models for comparison purposes. The former directly sums (with all coefficients set to 1) for reconstruction, while the latter employs the MLR method to optimize the reconstruction coefficients. Therefore, we constructed five distinct prediction models for the three time series and calculated their four evaluation indicators to compare and assess the proposed EEMD-LSTM-PSO model.

4. Results

4.1. Annual Runoff in Upper Reaches of Heihe River in China

EEMD finally decomposed the runoff data of Heihe River into 6 IMFs and a trend series (Figure 2). The curve of the residual item in Figure 2 reflects that there is an increasing trend in the annual runoff from 1800 to 2008. We build a prediction model for each decomposed component sequence following the LSTM modeling process described in the previous section. After repeated training and trials, we finally train an optimal LSTM model for each component sequence. Based on the prediction results of all component sequences, seven reconstruction coefficients need to be optimized. In the PSO algorithm, the population size is set to 500, the maximum number of iterations is 1000, and the mutation operation and linearly decreasing inertia weight are introduced. The optimal individual fitness value is calculated to be 9.4063, and the corresponding particle position is (1.2717, 0.9170, −1.8663, 2.2293, 1.5641, −0.0434, 0.9811). Therefore, the final predicted value can be calculated according to the following formula:

$$\begin{aligned} 1.2717 \cdot IMF_1 + 0.9170 \cdot IMF_2 - 1.8663 \cdot IMF_3 + 2.2293 \cdot IMF_4 \\ +1.5641 \cdot IMF_5 - 0.0434 \cdot IMF_6 + 0.9811 \cdot \text{Res} \end{aligned} \tag{11}$$

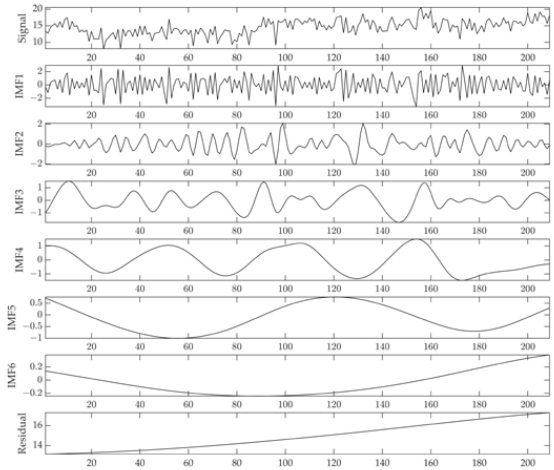

Figure 2. EEMD decomposition results of annual runoff.

Figure 3 shows the comparison of predicted and observed values, and the forecast error over 19 years for the EEMD-LSTM-PSO model. The RMSE is 0.70361 million m^3.

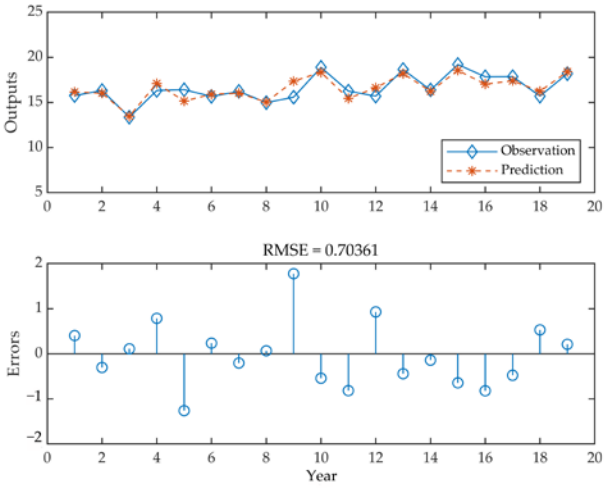

Figure 3. EEMD-LSTM-PSO prediction results of annual runoff.

4.2. Annual Average Precipitation in India

As mentioned previously, we use the first 126 items of the datasets to train the EEMD-LSTM-PSO model. After the EEMD process, five IMFs and one residual sequence are obtained (Figure 4). According to the residual in Figure 4, we can identify a decreasing trend in annual average precipitation in India. During the PSO process, the population size is set to 500 and the maximum number of iterations is set to 1000. And we introduced a mutation operation, to randomly update the particle swarm, and linearly decreasing inertia weight to update the particle velocity. The particle position corresponding to the optimal solution is calculated; that is, the reconstruction coefficient is (0.8665, 0.8206, −0.0795, −2.1811, 1.7403, 0.9868). So, the final predicted value can be calculated according to Formula (8):

$$\begin{array}{c} 0.8665 \cdot IMF_1 + 0.8206 \cdot IMF_2 - 0.0795 \cdot IMF_3 - 2.1811 \cdot IMF_4 \\ +1.7403 \cdot IMF_5 + 0.9868 \cdot \mathrm{Res} \end{array}, \quad (12)$$

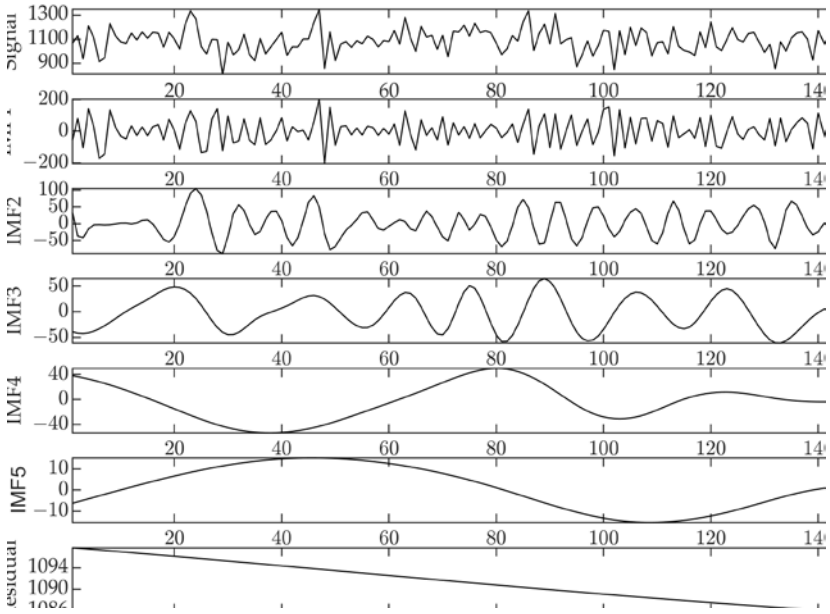

Figure 4. EEMD decomposition of annual mean precipitation data in India.

The outputs of the EEMD-LSTM-PSO model are the predictions of annual precipitation in India from 1997 to 2016 (Figure 5), of which the RMSE is 69.215 mm.

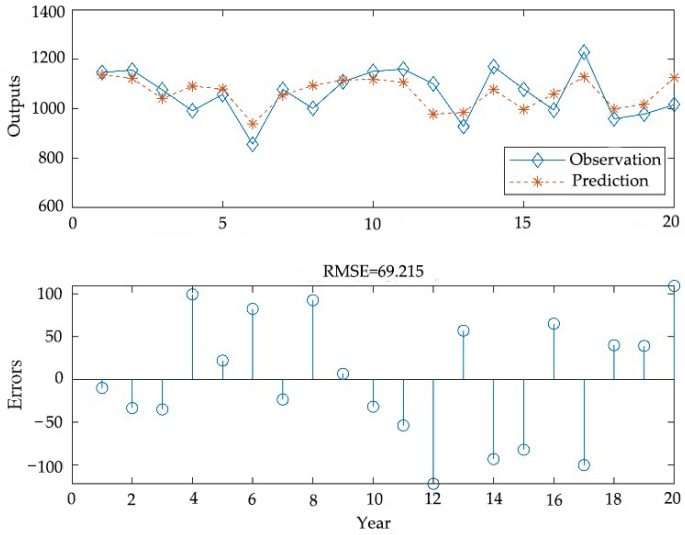

Figure 5. EEMD-LSTM-PSO prediction of annual precipitation in India.

4.3. Monthly Precipitation in Xilin River Basin in China

After EEMD decomposition, six IMFs and a trend series are obtained (Figure 6). From the change in the residual item, the precipitation in the Xinlin River basin shows a downward trend. Then, build an LSTM model for each of them. As a result, seven columns of prediction results are obtained, each column containing 36 data. Finally, the PSO algorithm is used to find the optimal combination coefficient. The population size is set to 500 and the maximum number of iterations to 10,000, introducing mutation operations and linearly decreasing inertia weights to the algorithm. The optimal individual fitness value is calculated to be 6338.2, and the corresponding particle position is (1.2834, 0.9325, 0.8232, 2.1044, 0.4627, −1.5787, 1.0275). Therefore, the final predicted value can be calculated according to the following formula:

$$\begin{aligned} &1.2834 \cdot IMF_1 + 0.9325 \cdot IMF_2 + 0.8232 \cdot IMF_3 + 2.1044 \cdot IMF_4 \\ &+0.4627 \cdot IMF_5 - 1.5787 \cdot IMF_6 + 1.0275 \cdot \text{Res} \end{aligned} \tag{13}$$

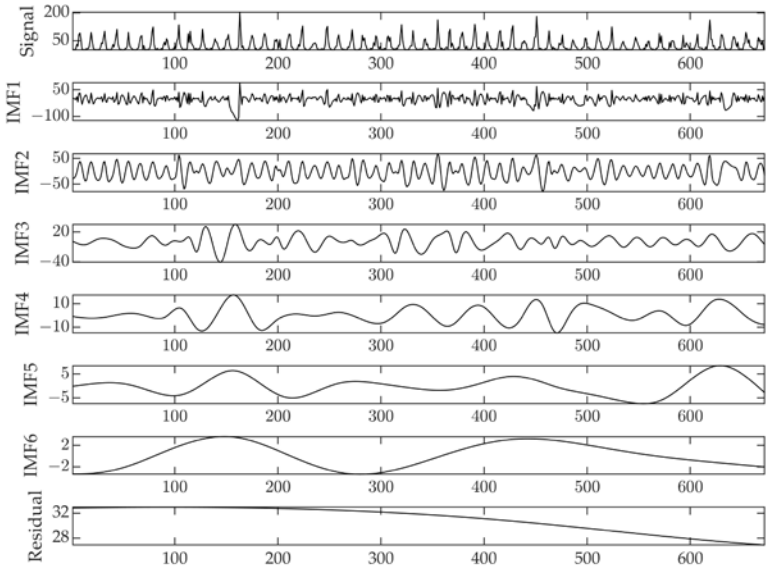

Figure 6. EEMD decomposition of monthly precipitation data in Xilin River Basin.

The prediction results of the model and the corresponding errors are showed in Figure 7. The red curve represents the predicted results and the blue curve represents the observed values. The predicted RMSE is 13.2918 mm.

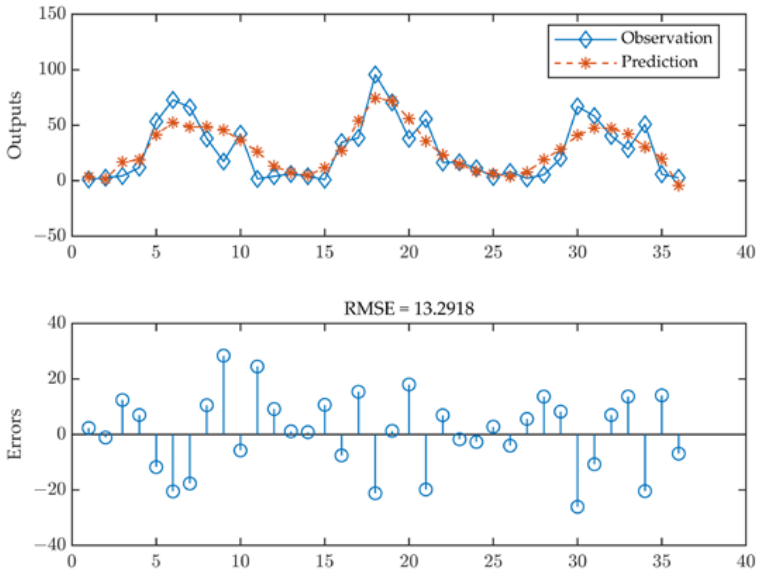

Figure 7. Prediction—and its errors—of monthly precipitation data in Xilin River Basin.

4.4. Model Comparation

To compare and analyze the effects of different models, we trained ARIMA, single LSTM, EEMD-LSTM, and EEMD-LSTM-MLR models on the three sequences while maintaining consistent data segmentation methods.

After undergoing the processes of model identification, model verification, and model refinement, we derived an ARIMA (1,1,2) for the runoff of the Heihe River, an ARIMA (1,0,1) for precipitation in India, and an ARIMA $(1,0,1)\times(0,0,1)_{12}$ for precipitation in Xilin River. The single LSTM model directly trains the LSTM without decomposing the sequence into columns. In contrast, EEMD-LSTM applies EEMD to decompose the sequence, trains an individual LSTM for each component obtained, and then aggregates the prediction results (with all coefficients set to 1) to obtain the overall prediction value. EEMD-LSTM-MLR utilizes the component prediction outcomes of EEMD-LSTM output and employs multiple linear regression (MLR) to optimize the reconstruction coefficients, thereby obtaining the ultimate prediction results.

After establishing models for the three datasets as described above, we calculated and summarized the four evaluation indicators of each model in Table 1. The ARIMA and LSTM models, when employed with the overall prediction strategy, exhibited inferior performance on the three series compared to the other three models utilizing the decomposition strategy. Among the three EEMD models, those utilizing reconstruction coefficient optimization exhibit superior performance, with EEMD-LSTM-PSO emerging as the most effective.

Table 1. Summary of model evaluation results.

Series	Models	RMSE	MAPE	R	NSE
Annual runoff	ARIMA	1.6472	6.94%	0.2302	−0.2996
	LSTM	2.1486	9.13%	0.2350	−1.2113
	EEMD-LSTM	1.1223	5.37%	0.8399	0.3966
	EEMD-LSTM-MLR	0.7074	3.47%	0.8569	0.7566
	EEMD-LSTM-PSO	0.7036	3.40%	0.8739	0.7629

Table 1. *Cont.*

Series	Models	RMSE	MAPE	R	NSE
Annual precipitation	ARIMA	97.0203	7.75%	−0.2445	−0.0992
	LSTM	97.8951	7.69%	0.1861	−0.1191
	EEMD-LSTM	78.3130	6.71%	0.5665	0.2838
	EEMD-LSTM-MLR	70.9189	5.93%	0.6333	0.4377
	EEMD-LSTM-PSO	69.2150	5.73%	0.6650	0.4406
Monthly precipitation	ARIMA	24.7653	294.54%	0.4356	0.0870
	LSTM	17.1164	67.29%	0.8098	0.5639
	EEMD-LSTM	13.7430	118.43%	0.8493	0.7189
	EEMD-LSTM-MLR	13.6609	116.66%	0.8526	0.7414
	EEMD-LSTM-PSO	13.2918	121.68%	0.8629	0.7445

5. Discussion

Time series forecasting has received a great deal of attention from researchers in the past few decades. This is due to the future need for and value of a physical variable in important planning, design, and management activities, which is measured in time on a discrete or continuous basis. Traditional time series modeling methods have served the scientific community for a long time. However, they suffer from stationarity and linearity assumptions. In recent years, the applicability of data-driven methods has become more popular than physical methods. The successful application of various data-driven models has opened a new space for the applicability of neural network time series analysis in the field of hydrometeorology.

A key hydrological variable is runoff at a location within a watershed. In many management and design activities of water resources, such as flood control and the management and design of various hydraulic structures (such as dams and bridges), it is very important to obtain an accurate flow forecast at a location in a river in a catchment. Runoff models that use only hydrological data are another forecasting model, except rainfall-runoff models, that use both climatic and hydrological data. Rainfall is another important hydrometeorological element. Its quantification is critical for the planning and management of water resources, and it is also used in the assessment of various parameters such as floods, droughts, runoff, agriculture, etc. Rainfall prediction is a challenging task due to the dynamic nature of climate phenomena [53].

EEMD can avoid modal aliasing and obtain more reasonable multi-scale components. LSTM has a good ability to predict high and low frequency components. Therefore, the LSTM model coupled with EEMD obtains the final prediction by directly superimposing the prediction results of each component. Compared with a variety of single prediction algorithms and traditional models, it can be found that the prediction effect is significantly improved. In many applications, such as short-term wind speed prediction [54], surface temperature prediction [55], stock index prediction [56], oil production prediction [57], etc., EEMD-LSTM has shown satisfactory prediction accuracy. The main reason for this may be that using the EEMD algorithm in the LSTM network can solve the hysteresis problem of its predictions. Because EEMD decomposes the time series into several component series, the details in the time series data are enlarged, and the fluctuation of each component series becomes more stable than the original series. However, in the time series prediction of hydrological and meteorological elements, the application research of the EEMD-LSTM model is still relatively rare. Therefore, this study focuses on the application and exploration of the EEMD-LSTM model in these aspects.

In the application of the EEMD-LSTM model, most researchers use a relatively simple result reconstruction method. The prediction results of the decomposed sequences are directly added to generate the final prediction. In the current research, we considered the reconstruction of the final prediction result by adopting a weighted summation method for the prediction of the decomposed component sequences. So, we added the optimization scheme of the weight coefficient. Considering that the PSO algorithm has the characteristics

of high speed, high reliability, and simplicity, we use it to optimize weight coefficients and compare it with multiple linear regression (MLR).

Our study considers three different types of hydrometeorological data sequences with different time scales and different dispersions in order to explore the performance of the EEMD-LSTM-PSO model. In the prediction experiment of the annual runoff in the upper reaches of the Heihe River, the effect of the EEMD-LSTM model is significantly improved compared with the single LSTM model. When PSO is introduced into the model, the prediction performance is further improved. RSME and MAPE are 0.7036 and 3.40%, respectively, which are 37.3% and 36.7% smaller than the EEMD-LSTM model, respectively. This shows that the introduction of a particle swarm optimization algorithm can effectively improve the prediction accuracy of EEMD-LSTM. The correlation coefficient R is increased to 0.8739, which is 0.034 more than the EEMD-LSTM model. Therefore, the addition of the PSO algorithm makes the change trend of the predicted results closer to the observed data. NSE improves from 0.3966 to 0.7629 for EEMD-LSTM. NSE closer to 1 indicates that the credibility of the model is improved and the quality is better.

We selected the precipitation data with the same scale as the previous experiment to conduct the experiment. The EEMD-LSTM-PSO model shows the same effect on the data series of annual mean precipitation in India. Compared with the EEMD-LSTM model, the four indicators of the EEMD-LSTM-PSO model achieved 11.6%, 14.6%, 18%, and 52.8% improvement, respectively, reaching 69.2150, 5.73%, 0.6650, and 0.4406.

In order to compare the effects of the EEMD-LSTM-PSO model on the time series of the same type of hydrometeorological elements at different time scales, we also conducted experiments using monthly precipitation data in the Xilin River Basin. It was found that the improvement in the prediction effect of EEMD on LSTM and PSO on EEMD-LSTM did not exceed the first two time series. Although the three evaluation indicators, RMSE, R, and NSE, have been gradually improved in the process of model improvement, another indicator, MAPE, which describes the accuracy of the model, has risen. However, we can still consider the EEMD-LSTM-PSO model to be the best according to the voting principle.

The coefficient of variation (CV) (the ratio of the standard deviation to the arithmetic mean) is a dimensionless metric that describes the degree of dispersion in the data. After calculation, the CV of the annual average precipitation data in India is 12.5%, while the precipitation series in the Xilin River Basin reaches 127.7%. Such a high CV reflects the great dispersion of the precipitation data series. The larger the CV of the series, the more difficult it is to predict. The reason for the large fluctuation of precipitation data in the Xilin River Basin is that the temporal distribution of precipitation in the basin is extremely uneven (for example, the precipitation in January 1991 was 1.3 mm, and in July 112.2 mm). Since the observations contain very small data (close to 0), slight fluctuations in the forecast results can cause a sharp rise in MAPE.

Although the EEMD-LSTM-PSO model exhibits a slightly better performance on the selected data, its generalization ability in terms of other regions and hydrometeorological elements (such as evaporation and wind speed) requires further investigation. Additionally, this paper's LSTM training process can be enhanced with intelligent techniques and hyperparameter tuning strategies, such as grid search random search. Regarding the signal decomposition method, this paper exclusively employs EEMD. However, it remains a question for future research whether alternative signal decomposition techniques can yield superior outcomes. With regards to the optimization of reconstruction coefficients, this paper solely compares multiple linear regression. However, future research could explore other optimization methods such as genetic algorithms and ant colony algorithms.

6. Conclusions

In this paper, we proposed an EEMD-LSTM-PSO model for the long-term prediction of hydrometeorological time series. This model employed the Ensemble Empirical Mode Decomposition (EEMD) technique to decompose hydrometeorological time series into simpler components, identified the optimal Long Short-Term Memory (LSTM) model

for each component, and subsequently utilized Particle Swarm Optimization (PSO) to determine the optimal weighted sum for generating accurate predictions. We conducted experiments on three datasets, namely the annual runoff of the Heihe River in China, the annual precipitation in India, and the monthly precipitation dataset of the Xilin River Basin in China. Additionally, we compared EEMD-LSTM-PSO with four other models based on four evaluation indicators: RSME, MAPE, R, and NSE. The results show that the proposed model outperforms the other four models in accurately predicting long-term hydrometeorological time series.

Author Contributions: Conceptualization, J.Z. and H.X.; methodology, G.W.; software, G.W.; validation, G.W., J.Z. and H.X.; formal analysis, G.W.; resources, H.X.; writing—original draft preparation, G.W.; writing—review and editing, J.Z. and H.X.; visualization, J.Z. All authors have read and agreed to the published version of the manuscript.

Funding: This research was funded by the Center for Applied Mathematics of Inner Mongolia (No. ZZYJZD2022002), the Interdisciplinary Research Fund of Inner Mongolia Agricultural University (No. BR231502), the Research Program of Science and Technology at the University of Inner Mongolia Autonomous Region (No. NJSY21477), the National Natural Science Foundation of China (No. 32160332), and the Inner Mongolia Agricultural University High-Level Talents Scientific Research Project (No. NDYB2019-35).

Institutional Review Board Statement: Not applicable.

Informed Consent Statement: Not applicable.

Data Availability Statement: Not applicable.

Conflicts of Interest: The authors declare no conflict of interest.

References

1. Şiir, K.; Goran, K.; Neven, D.; Rosen, M.A.; Moh'd, A.A. Effective mitigation of climate change with sustainable development of energy, water and environment systems. *Energy Convers. Manag.* **2022**, *269*, 116146.
2. Davide, A.G.; Giannakopoulos, D.; Predrag, R.; Neven, D.; Moh'd, A.A. Climate change mitigation by means of sustainable development of energy, water and environment systems. *Energy Convers. Manag.* **2023**, *17*, 100335.
3. Apel, H.; Abdykerimova, Z.; Agalhanova, M.; Baimaganbetov, A.; Gavrilenko, N.; Gerlitz, L.; Kalashnikova, O.; Unger-Shayesteh, K.; Vorogushyn, S.; Gafurov, A. Statistical forecast of seasonal discharge in Central Asia using observational records: Development of a generic linear modelling tool for operational water resource management. *Hydrol. Earth Syst. Sci.* **2018**, *22*, 2225–2254. [CrossRef]
4. Zhai, P.M.; Yuan, Y.F.; Yu, R.; Guo, G.P. Climate change and sustainable development for cities. *Chin. Sci. Bull.* **2019**, *64*, 1995–2001. [CrossRef]
5. Yang, X.; Maihemuti, B.; Simayi, Z.; Saydi, M.; Na, L. Prediction of Glacially Derived Runoff in the Muzati River Watershed Based on the PSO-LSTM Model. *Water* **2022**, *14*, 2018. [CrossRef]
6. Rakesh, V.; Goswami, P. An evaluation strategy of skill of high-resolution rainfall forecast for specific agricultural applications. *Meteorol. Appl.* **2016**, *23*, 529–540. [CrossRef]
7. Zscheischler, J.; Mahecha, M.D.; von Buttlar, J.; Harmeling, S.; Jung, M.; Rammig, A.; Randerson, J.T.; Schölkopf, B.; Seneviratne, S.I.; Tomelleri, E.; et al. A few extreme events dominate global interannual variability in gross primary production. *Environ. Res. Lett.* **2014**, *9*, 035001. [CrossRef]
8. Anderegg, W.R.L.; Trugman, A.T.; Badgley, G.; Konings, A.G.; Shaw, J. Divergent Forest sensitivity to repeated extreme droughts. *Nat. Clim. Chang.* **2020**, *10*, 1091–1095. [CrossRef]
9. Dannenberg, M.P.; Yan, D.; Barnes, M.L.; Smith, W.K.; Johnston, M.R.; Scott, R.L.; Biederman, J.A.; Knowles, J.F.; Wang, X.; Duman, T.; et al. Exceptional heat and atmospheric dryness amplified losses of primary production during the 2020 U.S. Southwest hot drought. *Glob. Chang. Biol.* **2022**, *28*, 4794–4806. [CrossRef]
10. Bao, A.M.; Liu, H.L.; Chen, X.; Pan, X.L. The effect of estimating areal rainfall using self-similarity topography method on the simulation accuracy of runoff prediction. *Hydrol. Process.* **2011**, *25*, 3506–3512. [CrossRef]
11. Huddart, B.; Subramanian, A.; Zanna, L.; Palmer, T. Seasonal and decadal forecasts of Atlantic Sea surface temperatures using a linear inverse model. *Clim. Dyn.* **2017**, *49*, 1833–1845. [CrossRef]
12. Khan, M.Z.K.; Sharma, A.; Mehrotra, R. Using all data to improve seasonal sea surface temperature predictions: A combination-based model forecast with unequal observation lengths. *Int. J. Climatol.* **2018**, *38*, 3215–3223. [CrossRef]
13. O'Dea, E.J.; Arnold, A.K.; Edwards, K.P.; Fumer, R.; Hyder, P.; Martin, M.J.; Siddorn, J.R.; Storkey, D.; While, J.; Holt, J.T.; et al. An operational ocean forecast system incorporating NEMO and SST data assimilation for the tidally driven European North-West shelf. *J. Oper. Oceanogr.* **2012**, *5*, 3–17. [CrossRef]

14. Mulungu, D.M.M.; Munishi, S.E. Simiyu River catchment parameterization using SWAT model. *Phys. Chem. Earth* **2007**, *32*, 1032–1039. [CrossRef]
15. Nijssen, B.; Schnur, R.; Lettenmaier, D.P. Global Retrospective Estimation of Soil Moisture Using the Variable Infiltration Capacity Land Surface Model, 1980–1993. *J. Clim.* **2001**, *14*, 1790–1808. [CrossRef]
16. Guo, F.; Liu, X.R.; Ren, L.L. A Topography Based Hydrological Model: TOPMODEL and Its Widened Application. *Adv. Waterence* **2000**, *11*, 296–301.
17. Devia, G.K.; Ganasri, B.P.; Dwarakish, G.S. A Review on Hydrological Models. *Aquat. Procedia* **2015**, *4*, 1001–1007. [CrossRef]
18. Eddine, B.I.; Guastaldi, E.; Zirulia, A.; Brancale, M.; Bengusmia, D. Trend analysis and spatiotemporal prediction of precipitation, temperature, and evapotranspiration values using the ARIMA models: Case of the Algerian Highlands. *Arab. J. Geosci.* **2021**, *13*, 1281.
19. Zhang, Y.; Yang, H.; Cui, H.; Chen, Q. Comparison of the Ability of ARIMA, WNN and SVM Models for Drought Forecasting in the Sanjiang Plain, China. *Nat. Resour. Res.* **2019**, *29*, 1447–1464. [CrossRef]
20. Dhote, V.; Mishra, S.; Shukla, J.P.; Pandey, S.K. Runoff prediction using big data analytics based on ARIMA model. *Indian J. Geo-Mar. Sci.* **2018**, *47*, 2163–2170.
21. Demirel, M.C.; Venancio, A.; Kahya, E. Flow forecast by SWAT model and ANN in Pracana basin, Portugal. *Adv. Eng. Softw.* **2009**, *40*, 467–473. [CrossRef]
22. Sohail, A.; Watanabe, K.; Takeuchi, S. Stream flow forecasting by artificial neural network (ANN) model trained by real coded genetic algorithm (GA). *J. Groundw. Hydrol.* **2006**, *48*, 233–262.
23. Hung, N.Q.; Babel, M.S.; Weesakul, S.; Tripathi, N.K. An artificial neural network model for rainfall forecasting in Bangkok, Thailand. *Hydrol. Earth Syst. Sci.* **2009**, *13*, 1413–1425. [CrossRef]
24. Wu, C.L.; Chau, K.W.; Fan, C. Prediction of rainfall time series using modular artificial neural networks coupled with data-preprocessing techniques. *J. Hydrol.* **2010**, *389*, 146–167. [CrossRef]
25. Han, S.; Liu, Y.; Yang, Y. Taboo Search Algorithm Based ANN Model for Wind Speed Prediction. In Proceedings of the IEEE Conference on Industrial Electronics & Applications, Harbin, China, 23–25 May 2007.
26. Sulaiman, M.; El-Shafie, A.; Karim, O.; Basri, H. Improved Water Level Forecasting Performance by Using Optimal Steepness Coefficients in an Artificial Neural Network. *Water Resour. Manag.* **2011**, *25*, 2525–2541. [CrossRef]
27. Hochreiter, S.; Schmidhuber, J. Long Short-Term Memory. *Neural Comput.* **1997**, *9*, 1735–1780. [CrossRef]
28. Ma, X.; Tao, Z.; Wang, Y.; Yu, H.; Wang, Y. Long short-term memory neural network for traffic speed prediction using remote microwave sensor data. *Transp. Res. Part C Emerg. Technol.* **2015**, *54*, 187–197. [CrossRef]
29. Kratzert, F.; Klotz, D.; Brenner, C.; Schulz, K.; Herrnegger, M. Rainfall–runoff modelling using Long Short-Term Memory (LSTM) networks. *Hydrol. Earth Syst. Sci.* **2018**, *22*, 6005–6022. [CrossRef]
30. Widiasari, I.R.; Nugoho, L.E.; Widyawan; Efendi, R. Context-based Hydrology Time Series Data for a Flood Prediction Model Using LSTM. In Proceedings of the 2018 5th International Conference on Information Technology, Computer, and Electrical Engineering (ICITACEE), Semarang, Indonesia, 27–28 September 2018.
31. Xiang, Z.; Yan, J.; Demir, I. A Rainfall-Runoff Model With LSTM-Based Sequence-to-Sequence Learning. *Water Resour. Res.* **2020**, *56*, e2019WR025326. [CrossRef]
32. Holden, K.; Peel, D.A. An empirical investigation of combinations of economic forecasts. *J. Forecast.* **1986**, *5*, 229–242. [CrossRef]
33. Wu, Z.; Huang, N.E. Ensemble empirical mode decomposition: A noise-assisted data analysis method. *Adv. Adapt. Data Anal.* **2011**, *1*, 1–41. [CrossRef]
34. Wang, W.C.; Chau, K.W.; Xu, D.M.; Chen, X.Y. Improving Forecasting Accuracy of Annual Runoff Time Series Using ARIMA Based on EEMD Decomposition. *Water Resour. Manag.* **2015**, *29*, 2655–2675. [CrossRef]
35. Wang, W.C.; Chau, K.W.; Qiu, L.; Chen, Y.B. Improving forecasting accuracy of medium and long-term runoff using artificial neural network based on EEMD decomposition. *Environ. Res.* **2015**, *139*, 46–54. [CrossRef] [PubMed]
36. Bazi, Y.; Melgani, F. Semisupervised PSO-SVM regression for biophysical parameter estimation. *IEEE Trans. Geosci. Remote Sens.* **2007**, *45*, 1887–1895. [CrossRef]
37. Melin, P.; Olivas, F.; Castillo, O.; Valdez, F.; Soria, J.; Valdez, M. Optimal design of fuzzy classification systems using PSO with dynamic parameter adaptation through fuzzy logic. *Expert Syst. Appl.* **2013**, *40*, 3196–3206. [CrossRef]
38. Liu, Z.H.; Wei, H.L.; Li, X.H.; Liu, K.; Zhong, Q.C. Global Identification of Electrical and Mechanical Parameters in PMSM Drive based on Dynamic Self-Learning PSO. *IEEE Trans. Power Electron.* **2018**, *33*, 10858–10871. [CrossRef]
39. Huang, N.E.; Shen, Z.; Long, S.R.; Wu, M.C.; Shih, H.H.; Zheng, W.; Yen, N.; Tung, C.C.; Liu, H.H.; Yen, N.C. The empirical mode decomposition method and the Hilbert spectrum for non-stationary time series analysis. *Proc. Math. Phys. Eng. Sci.* **1998**, *454*, 903–998. [CrossRef]
40. He, J.B.; Peng, F.Y. Algorithm for image compression based on improved EMD. *J. Infrared Millim. Waves* **2008**, *27*, 295–298.
41. Bharathi, B.M.R.; Mohanty, A.R. Underwater Sound Source Localization by EMD-Based Maximum Likelihood Method. *Acoust. Aust.* **2018**, *46*, 193–203. [CrossRef]
42. Chen, Y.K.; Zhou, C.; Yuan, J.; Jin, Z.Y. Applications of Empirical Mode Decomposition in random noise attenuation seismic data. *J. Seism. Explor.* **2014**, *23*, 481–495.
43. Martins, L.; Miller, S.D.; Ac Evedo, O.C. Using Empirical Mode Decomposition to Filter Out Non-turbulent Contributions to Air–Sea Fluxes. *Bound.-Layer Meteorol.* **2017**, *163*, 123–141. [CrossRef]

44. Srivastava, S.; Lessmann, S. A comparative study of LSTM neural networks in forecasting day-ahead global horizontal irradiance with satellite data. *Sol. Energy* **2018**, *162*, 232–247. [CrossRef]
45. Meng, X.; Yang, T. Entanglement-Structured LSTM Boosts Chaotic Time Series Forecasting. *Entropy* **2021**, *23*, 1491. [CrossRef] [PubMed]
46. Graves, A. Generating Sequences with Recurrent Neural Networks. *arXiv* **2013**, arXiv:1308.0850.
47. Kennedy, J.; Eberhart, R. Particle Swarm Optimization. In Proceedings of the ICNN'95-international Conference on Neural Networks, Perth, WA, Australia, 27 November–1 December 1995.
48. Shi, Y.H.; Eberhart, R.C. Empirical study of particle swarm optimization. In Proceedings of the Congress on Evolutionary Computation, Washington, DC, USA, 6–9 July 2002.
49. Chang, Z.H.; Zhang, Y.; Chen, W.B. Electricity price prediction based on hybrid model of adam optimized LSTM neural network and wavelet transform. *Energy* **2019**, *187*, 115804. [CrossRef]
50. Mielke, P.W.; Berry, K.J. Euclidean Distance Based Permutation Methods in Atmospheric Science. *Data Min. Knowl. Discov.* **2000**, *4*, 7–27. [CrossRef]
51. Shi, Y. A Modified Particle Swarm Optimizer. In *1998 IEEE International Conference on Evolutionary Computation Proceedings, Proceedings of the IEEE World Congress on Computational Intelligence (Cat. No.98TH8360), Anchorage, AK, USA, 4–9 May 1998*; IEEE: Piscataway, NJ, USA, 1998.
52. Nash, J.E.; Sutcliffe, J.V. River flow forecasting through conceptual models part I—A discussion of principles-ScienceDirect. *J. Hydrol.* **1970**, *10*, 282–290. [CrossRef]
53. Kumar, D.; Singh, A.; Samui, P.; Jha, R.K. Forecasting monthly precipitation using sequential modelling. *Hydrol. Sci. J.-J. Sci. Hydrol.* **2019**, *64*, 690–700. [CrossRef]
54. Kang, A.; Tan, Q.; Yuan, X.; Lei, X.; Yuan, Y. Short-Term Wind Speed Prediction Using EEMD-LSSVM Model. *Adv. Meteorol.* **2017**, *2017*, 6856139. [CrossRef]
55. Zhang, X.; Zhang, Q.; Zhang, G.; Nie, Z.; Gui, Z.; Que, H. A Novel Hybrid Data-Driven Model for Daily Land Surface Temperature Forecasting Using Long Short-Term Memory Neural Network Based on Ensemble Empirical Mode Decomposition. *Int. J. Environ. Res. Public Health* **2018**, *15*, 1032. [CrossRef]
56. Yujun, Y.; Yimei, Y.; Jianhua, X. A Hybrid Prediction Method for Stock Price Using LSTM and Ensemble EMD. *Complexity* **2020**, *2020*, 6431712. [CrossRef]
57. Liu, W.; Liu, W.D.; Gu, J. Forecasting oil production using ensemble empirical model decomposition based Long Short-Term Memory neural network. *J. Pet. Sci. Eng.* **2020**, *189*, 107013. [CrossRef]